Self-Regulation Phenomena Applied to Bacterial Reaction Centers 2. Nonequilibrium Adiabatic Potential: Dark and Light Conformations Revisited

Alexander O. Goushcha,*† Anthony J. Manzo,* Gary W. Scott,* Leonid N. Christophorov,†‡ Peter P. Knox,§ Yuri M. Barabash,† Marina T. Kapoustina,† Natalja M. Berezetska,† and Valery N. Kharkyanen†

*Department of Chemistry, University of California/Riverside, Riverside, California; †Institute of Physics, National Academy of Science of Ukraine, Kyiv, Ukraine; ‡Bogoliubov Institute for Theoretical Physics, National Academy of Science of Ukraine, Kyiv, Ukraine; and §Lomonosov Moscow State University, Moscow, Russia

ABSTRACT Experimental and theoretical results in support of nonlinear dynamic behavior of photosynthetic reaction centers under light-activated conditions are presented. Different conditions of light adaptation allow for preparation of reaction centers in either of two different conformational states. These states were detected both by short actinic flashes and by the switching of the actinic illumination level between different stationary state values. In the second method, the equilibration kinetics of reaction centers isolated from *Rhodobacter sphaeroides* were shown to be inherently biphasic. The fast and slow equilibration kinetics are shown to correspond to electron transfer (charge separation) at a fixed structure and to combined electron-conformational transitions governed by the bounded diffusion along the potential surface, respectively. The primary donor recovery kinetics after an actinic flash revealed a pronounced dependence on the time interval (Δt) between cessation of a lengthy preillumination of a sample and the actinic flash. A pronounced slow relaxation component with a decay half time of more than 50 s was measured for $\Delta t > 10$ s. This component corresponds to charge recombination in reaction centers for which light-induced structural changes have not relaxed completely before the flash. The amplitude of this component depended on the conditions of the sample preparation, specifically on the type of detergent used in the preparation. The redox potential parameters as well as the structural diffusion constants were estimated for samples prepared in different ways.

INTRODUCTION

As is well known, redox proteins have sufficient conformational flexibility to actively influence the electron transfer rate (see e.g., the recent review by Warshel and Parson, 2001.). In the early 1990s, it was proposed that regulation of elementary processes in biological systems, at the molecular level, might be dynamic and self-organizational (Chinarov et al., 1992; Christophorov et al., 1992; Gushcha et al., 1994; Tributsch and Pohlmann, 1992; Tributsch and Bogomolni, 1994), analogous to what occurs when light propagates in an active media (Haken, 1983; Nicolis and Prigogine, 1977). There are two key events here, one is the *flow* of charged species, i.e., many sequential, elementary reaction steps occurring in the molecule. The other is the *control* by slowly relaxing structural modes of the protein and cofactors. The protein assumes an active feedback role on protein structural changes caused by the flow, modifying the flow efficiency. The idea for dynamic self-organization in charge transfer biomolecules was developed recently in the literature (Tributsch and Pohlmann, 1998; Goushcha et al., 1999, 2000; Christophorov et al., 2000). A strong, charge-conformational interaction in combination with considerable flexibility of the protein matrix promotes nonequilibrium regimes involving formation of functionally important conformational states. The formalism describing this phenomenon was based on a stochastic theory of multiple, sequential electron transfer events that are correlated with slow structural motions in biological macromolecules. This formalism is very similar to the well-known approach by Agmon and Hopfield (1983) insofar as the conformational motions of protein are treated as a drift and diffusion along some single ''perpendicular coordinate'' (see e.g., Christophorov et al., 2000). However, the work by Agmon or other researchers, in which they explored many consecutive turnovers of the protein, does not discuss the possibility of a dynamic self-organization in the system with a threshold-like emergence of new, equilibrium functional states (see e.g., Agmon and Krissinel, 1998; Agmon, 2000; McMahon et al., 1998). Nevertheless, such an effect is virtually inevitable in nonlinear systems with external fluxes (Haken, 1983). A conventional approach (see above) uses structural potentials that correspond to different redox states of the cofactors. In contrast, for the case of slow conformational modes, the effective, adiabatic nonequilibrium potential is physically more appropriate because it accounts for the dynamics of redistribution of the cofactors' electronic state populations (see Christophorov et al., 2000; Goushcha et al., 2000 for details). Most importantly, the shape of this potential is controlled by the intensity of the photon flux, resulting in a very powerful method of (self-) regulation of the functional activity of proteins. Recent studies showed that a similar approach based on an adiabatic separation between the reaction coordinate and the remaining degrees of freedom may be very fruitful in molecular dynamic

Submitted June 7, 2002, and accepted for publication September 27, 2002.

Address reprint requests to Gary W. Scott, E-mail: GaryScott@citrus.ucr.edu; or Alexander O. Goushcha, Fax: +909-787-4713; E-mail: goushcha@ucrac1.ucr.edu.

0006-3495/03/02/1146/15 $2.00

simulations of rare events in biomolecules (Rosso et al., 2002).

In Part 1 of these studies, the synergetic effects caused by light-induced structural changes in photosynthetic reaction centers (RCs) were described theoretically (Goushcha et al., 2000). In the present work, we present experimental evidence, accompanied by computer modeling, in support of this theory. The main emphasis is on changes in the effective adiabatic potential caused by a stepwise variation of the exciting light intensity. We explore the correlation between the appearance and further modification of the ''light'' conformational state and the kinetics of light-induced absorption changes in RCs. These correlations are well described by structural diffusion on the effective adiabatic potential.

Experimental observation of dynamic, nonequilibrium effects is often obscured by complex relaxation/dissipation processes that occur in response to the creation of a nonequilibrium state (see e.g., Carpintero and Lamela, 2000). This problem also occurs in the experimental verification of structural regulation mechanisms in proteins, in which the inherent complexity significantly complicates a direct monitoring of the protein structural relaxation in different redox states (van Mourik et al., 2001; Barabash et al., 2002). Thus, in the present work, we present experimental results that confirm the existence of the protein structural memory that lasts for a time longer than the interval between consecutive turnovers of the reaction center—a necessary condition for the nonlinear self-organization mechanisms in the ET system of an RC.

In this work, we used different detergents for RC sample preparation. Detergents are crucial for solubilization of proteins. In isolated RCs, detergent molecules are tightly bound to the protein, effectively influencing the function of biomolecules (see e.g., Feher and Okamura, 1978; Gast et al., 1996). In particular, detergents affect protein secondary structure (Ruan et al., 2000), crystallization properties of the protein (Hoff and Deisenhofer, 1997; Michel, 1991; Marone et al., 1999), the thermodynamics of quinone exchange (Shinkarev and Wraight, 1997; Agostiano et al., 1999), electron transfer kinetics (Gast et al., 1996; Tiede et al., 1996, 1998), and proton uptake (Valerio-Lepiniec et al., 1997). This work addresses, for the first time, the effects of detergents on nonlinear dynamic properties of RCs.

MATERIALS AND METHODS

Samples

In experimental studies, we used isolated RCs from photosynthetic bacteria *Rhodobacter (Rb.) sphaeroides*, wild-type and strain R26. These RCs were isolated and purified from photosynthetic membranes using the detergent lauryl-N,N,-dimethylamine-N-oxide (LDAO) according to the procedure described previously (Feher and Okamura, 1978; Zakharova et al., 1981). After purification in a column with oxiapatite, RCs were suspended in 10 mM Tris-HCl buffer with 0.05% LDAO, pH 7.5. Two other solutions of RCs were obtained by dialysis against an excess of two different detergents, Triton X-100 (0.05%, pH 7.5) and sodium (Na) cholate (0.1%, pH 8.0), respectively, according to conventional methods (see Zakharova and Churbanova, 2000; Lin et al., 2001 for more details about sample preparation). Note that, in contrast to LDAO, which is a zwitterionic detergent, Triton X-100 is a nonionic detergent and Na cholate is an anionic detergent. Different ionic properties of the three different detergents should affect in different ways the electrostatic environment of the protein, thereby influencing its function. The occupancy of the Q_B site after the isolation procedure was 30–90% (measured by the slow phase amplitude in the charge recombination kinetics after a saturating flash). No quinone reconstitution procedure was used. The samples were checked for the absence of cytochrome c2, assuring that each RC could undergo only one-electron photoactivation in our experiments. The absorbance ratio A_{280}/A_{800} that characterizes the sample purity was usually 1.25–1.35.

Experimental setup

Experiments were made using an optical setup designed in our laboratory. We placed sample solutions in either a 4-mm or a 10-mm pathlength quartz cuvette. The steady-state optical absorbance of the samples was adjusted to be within the range $A_{800} = 0.4$–0.5. The probe beam was provided either by a tungsten-halogen lamp filtered with the grating monochromator ($\lambda = 865$ nm) or by a red light emitting diode (LED) with a maximum optical power centered at 835 nm. The probe beam ($I_{test} < 0.1$ μW/cm^2) transmitted through the sample was filtered either with another monochromator or with band pass filters and recorded with an Si photodiode coupled to a lock-in amplifier. In the apparatus using a probe beam from a tungsten-halogen lamp, the beam was chopped at a frequency 1350 Hz. In the other apparatus, the LED provided a probe beam modulated at 50 kHz. The preamplifier bandwidth was at least 10 times larger than the frequency of modulation and the sampling rate in each experiment was at least 100 times slower than this frequency.

The pulsed photoexcitation of a sample was provided by four LEDs ($\lambda_{max} = 835$ nm) with a total maximum power at the sample of 3.5 mW/cm^2, well above the half-saturation limit for the bacterial RCs. The pulse duration was either 100 or 400 ms. The absorbance recovery kinetics, measured after single pulsed photoexcitation of the RCs, was exactly the same as in the case of photo-flash excitation of RCs with a single strong 2-ms light pulse.

The additional background, continuous wave (cw) excitation of the sample was provided by either a tungsten-halogen lamp filtered with red cut-off filters and an interference filter ($\lambda_{max} = 850$ nm) or by four LEDs ($\lambda_{max} = 835$ nm). The photoexcitation beam crossed the measuring light beam at an angle of either 45° or 90°. Care was taken to ensure a homogeneous excitation level across the cuvette surface. The photoexcitation intensity was adjusted using a set of neutral density filters in the case of the tungsten-halogen lamp. The irradiation intensity of the LEDs was controlled by adjusting the power supply current. The maximum excitation flux was ~3.5 mW/cm^2.

The intensities of the probe beam and the background excitation light were monitored simultaneously as was the light that was transmitted through the sample, to account for possible instabilities in the light sources. The cuvette temperature was stabilized at either 23 ± 0.5°C or 4 ± 0.5°C. Data collection and experimental control was provided by a PC with a plug-in data acquisition board.

Theoretical model

In modeling of the experimental results, we utilized the phenomenological theory described in detail previously (Goushcha et al., 2000; Christophorov et al., 2000). The calculation of RC absorption changes with variation of actinic light intensity were based on the forward Kolmogorov equations for a reduced two-level scheme of RC redox states:

$$\frac{\partial P_P(t,x)}{\partial t} = L_P P_P(t,x) - I P_P(t,x) + k_{AP} e^{-x} P_B(t,x)$$
$$\frac{\partial P_B(t,x)}{\partial t} = L_B P_B(t,x) + I P_P(t,x) - k_{AP} e^{-x} P_B(t,x), \qquad (1)$$
$$L_i = D_i \frac{\partial}{\partial x}\left(\frac{dV_i(x)}{dx} + \frac{\partial}{\partial x}\right),\ x = \frac{\Delta G_{AB}}{k_B T},\ i = P, B$$

in which $P_P(t,x)$ and $P_B(t,x)$ describe the time evolution of the RC distribution function over a single dimensionless structural variable x in two different redox states, PQ_AQ_B (neutral state) and $P^+Q_AQ_B^-$ (charge separated state), respectively. I stands for the photoexcitation intensity, in units of the rate of a single RC photoexcitation, and k_{AP} is the rate of electron recombination from the primary quinone acceptor Q_A to pigment P (the photoelectron donor, which is the bacteriochlorophyll dimer). The rate of electron recombination from the secondary quinone acceptor Q_B is $k_{AP}e^{-x}$; D_i is the diffusion constant; ΔG_{AB} is the difference of the quasi free energies for electron localization either on Q_A or on Q_B; k_B is the Boltzmann constant; T is an absolute temperature; V_P, V_B, and x_P, x_B are the redox potentials in k_BT units and their minima positions for the charge neutral (index P) and charge-separated (index B) states of RCs, respectively.

We have shown previously that those structural rearrangements that occur more slowly than the electronic transitions that initiate them might be correctly described using a light intensity controlled, nonequilibrium adiabatic potential $V_I^{eff}(x)$ (see Fig. 1). This potential is determined from the equation

$$\frac{dV_I^{eff}(x)}{dx} = \frac{dV_P(x)}{dx}\rho_P^{st}(x;I) + \frac{dV_B(x)}{dx}\rho_B^{st}(x;I), \qquad (2)$$

in which $\rho_P^{st}(x;I) = (k_{AP}e^{-x})/(I + k_{AP}e^{-x})$, $\rho_A^{st}(x;I) = I/(I + k_{AP}e^{-x})$ are the stationary state populations of the electronic states at a fixed value of the structural variable x and given photoexcitation intensity I. Equation 2 describes the contribution that the slow structural variable experiences from an average force arising from fast transitions of the photoactivated electron between redox cofactors. This force integrates contributions from each redox potential with the weight that corresponds to the average survival time for the photoelectron on each redox cofactor. Therefore, the motion equation for the structural variable x in the adiabatic approximation can be written as follows:

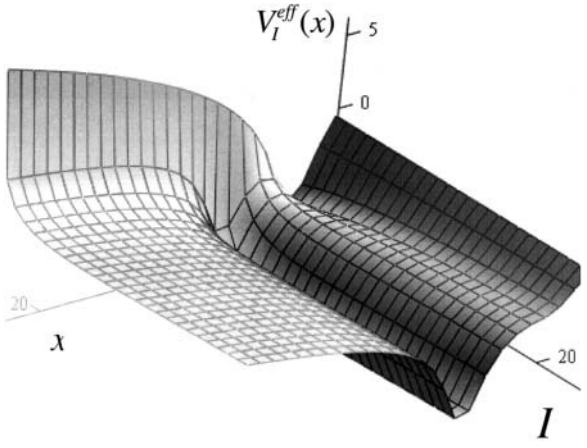

FIGURE 1 RC effective adiabatic potential $V_I^{eff}(x)$. The redox potentials were chosen in the form of Eq. 4. The model parameters were the following: $x_P = 2$; $x_B = 8$; $k_P = 10$; $k_B = 10$; $\alpha_P = \alpha_B = 0.07$; $\gamma_P = \gamma_B = 1.1$; and $k_{AP} = 10\ s^{-1}$. See text for more details.

$$\frac{\partial P(t;x)}{\partial t} = D\frac{\partial}{\partial x}\left[\frac{1}{k_B T}\frac{\partial V_I^{eff}(x)}{\partial x}P(t;x) + \frac{\partial P(t;x)}{\partial x}\right], \qquad (3)$$

in which $P(t;x) = \sum_i P_i(t;x)$ is the distribution function density for the structural variable. The stationary state solution of Eq. 3 reads $P(\infty;x) = e^{-V_I^{eff}(x)/k_BT}/z(I)$, in which $z(I) = \int dx \cdot e^{-V_I^{eff}(x)/k_BT}$.

The effective conformational potential has been discussed previously for the case of harmonic redox potentials $V_P(x)$ and $V_B(x)$ (Goushcha et al., 1997b, 1999, 2000), but the detailed consideration of its application to the description of structural rearrangements caused by instantaneous variation in the actinic light intensity has never been evaluated. Such a description is made in the present work employing realistic redox potentials of RCs.

In general, the choice of a redox potential to describe slow structural motions of a molecule is very specific for each particular molecule. In many cases, for a single well potential, the harmonic approximation suffices, thus describing an elastic restoring force. For example, the harmonic approximation was successfully applied to a description of the structural variable (perpendicular coordinate) dynamics in sorption/desorption processes of carbon monoxide in myoglobin (Agmon and Hopfield, 1983; Agmon and Krissinel, 1998). Such an approximation is clearly justified for small shifts of the structural variable from its equilibrium. In contrast, for large shifts, anharmonic processes may completely dominate system behavior.

The modeling of RC structural dynamics that accompanies photoinduced charge separation and electron transfer along the chain of cofactors that we reported recently showed that harmonic potentials do not provide a correct description of RC slow structural dynamics for any set of parameters. For example, the experimentally measured width of a hysteresis loop for the absorption changes versus actinic light intensity was always considerably larger than that calculated using a harmonic potential approach (Gushcha et al., 1994; Goushcha et al., 1997a). In several cases, the divergent or convergent behavior of RC stationary-state absorbance changes in response to a sequence of repetitive alternations of cw actinic light intensity between two levels within the bistability domain was measured (Goushcha et al., 1999). The type of absorption change behavior observed could be readily modeled using anharmonic redox potentials. In evaluating potentials of different complexity, we assumed that the restoring force might be considered as elastic (k_i—the elasticity constant) inside a certain interval of small shifts of the structural variable from its equilibrium position. Outside this interval the elastic portion of the force was assumed to vanish smoothly, preserving the overall symmetric form with respect to the equilibrium position x_i:

$$V_i(x) = \frac{1}{2}k_i(x - x_i)^{2(1+\alpha_i)}\frac{\gamma_i}{\gamma_i^2 + (x - x_i)^2}. \qquad (4)$$

The width of the interval, over which the potential can be considered as harmonic, is determined by the parameter γ_i: $V_i(x) \approx (k_i/2\gamma_i)(x - x_i)^2$ for $|x - x_i| \le \gamma_i$ and $\alpha_i < 1$. In the opposite case, for $|x - x_i| > \gamma_i$, the potential $V_i(x) \approx (k_i\gamma_i/2)(x - x_i)^{2\alpha}$ is anharmonic and the degree of anharmonicity is determined by the parameter α_i. The anharmonic potential given by Eq. 4 allows for very good agreement between the modeling results and experiment (see e.g., Barabash et al., 2002). It describes well the bleaching and recombination kinetics of photoexcited RCs at various exposure times, enabling also determination of the parameters α_i and γ_i.

Fig. 2 shows transmission bleaching and dark recovery kinetics for the P band of *Rb. sphaeroides* RCs (suspended in buffer containing 0.1% Na cholate) at 4°C measured after turning on and off a cw actinic light (3.5 mW/cm^2). The exposure time was varied from 5 to 200 s. A well-defined slow relaxation component was always detected in such experiments. The dashed lines in Fig. 2 show the results of modeling the experimental curves with Eqs. 1–3 using the redox potentials in the form of Eq. 4. The method of computing the time-dependent populations of RC cofactors is given elsewhere (Barabash et al., 2002). The theoretical formalism for calculation of a generalized conformational potential at an arbitrary actinic light intensity is given in our previous work (Goushcha et al., 1997a, 2000;

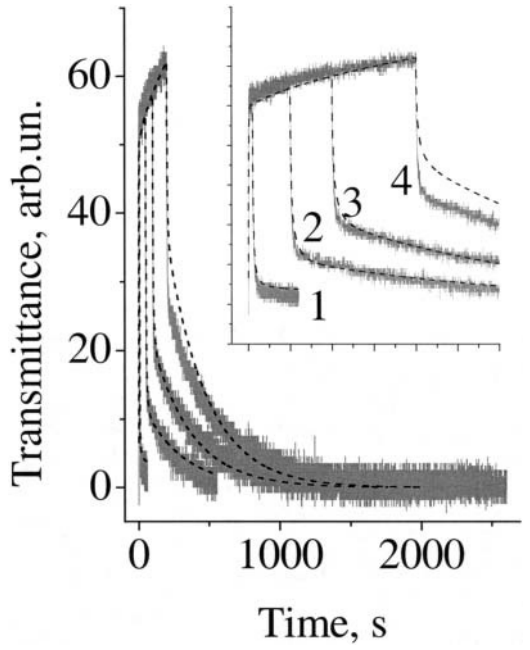

FIGURE 2 RC bleaching and recovery kinetics measured in the primary electron donor P absorption band. The actinic light intensity was 3.5 mW/cm^2 and exposure time was 5 s (*curve 1*), 50 s (*curve 2*), 100 s (*curve 3*), and 200 s (*curve 4*). $\lambda_{exc} = 835$ nm. The dashed lines show the modeling results. (*Inset*) The initial parts of the curves. Experimental conditions: 0.7 μM RC in the buffer 20 mM Tris-HCl, pH 8.0, and 0.1% Na cholate; ~80% of Q_B-active RCs and no quinone reconstitution procedure was applied; $T = 4$°C.

Abgaryan et al., 1998). The RCs transmittance at 865 nm and at photoexcitation intensity I was calculated by computing the time-dependent population of the charge-separated state $n_B(t)$:

$$n_B(t) = \int P_B(x,t)dx \approx \int dx \cdot \left\{ \frac{I}{I + k_{AP}e^{-x}} + \left[n_B(0) - \frac{I}{I + k_{AP}e^{-x}} \right] e^{-(I+k_{AP}e^{-x})t} \right\} \cdot P(t,x), \quad (5)$$

assuming that only the special pair absorbs at 865 nm. The approximate equality in Eq. 5 indicates that the right-hand side expression in Eq. 5 is valid in the adiabatic approximation. This expression allows numeric calculation of both the fast and slow components of the photoexcitation kinetics (increasing signal) in Fig. 2. In particular, the faster process with the characteristic time constant $\tau_{el}(x, I) = (I + k_{AP}e^{-x})^{-1}$ describes the kinetics of establishing quasiequilibrium electronic populations of the cofactors at a fixed value of the generalized structural variable x, whereas the slower process corresponds to the bounded diffusion of the probability density function $P(t,x)$ on the nonequilibrium adiabatic potential as described by Eq. 3. As it is seen in Fig. 2, the increasing part of all curves has two well-defined kinetic phases as predicted by the adiabatic relationship Eq. 5. The decreasing part of all curves in Fig. 2 describes the charge recombination process and was measured upon turning off the photoactivation. This part also has two pronounced relaxation phases, but they cannot be described by an adiabatic theory because $\tau_{el}(x, 0)$ may become quite long at large x due to large light-induced deformation (structural changes). These values of $\tau_{el}(x, 0)$ may be comparable to the characteristic time of slow structural rearrangement of the macromolecule. In this case, the recombination process may be viewed as a mixed electron-conformational relaxation process wherein its biphasicity evidences the bistability in the system.

In the present work, the conformational potentials for the neutral and the charge-separated states were chosen in the form of Eq. 4, and the parameter values that gave the best fit to the experimental curves are given in Table 1. The photoexcitation intensity $I = 2$ s^{-1} was turned on at time $t = 0$, and the sampling time was 0.05 s (see Fig. 2).

The fitting parameters were identical for samples with Triton X-100 buffer and for samples with a Na cholate buffer at 23°C. The diffusion constants were found to be considerably larger for the sample with an LDAO buffer than for the two other samples. Our recent studies showed that the theoretical parameter that controls the structural memory extent is primarily the diffusion constant D_P (Barabash et al., 2002). RC samples prepared with different detergents often reveal different dynamic properties; therefore, different values for the diffusion constants D_P and D_B as well as for the elastic constants k_B and k_P, as determined here for the three samples, are not a surprising result and this correlates well with a variety of studies into RC dynamics.

The ability to model the experimental results was very good for short and medium exposure times (see *curves 1–3* in Fig. 2), but it was not as good for long exposure times (see *curve 4* in Fig. 2). Some possible reasons for this difference will be addressed in Discussion section.

RESULTS

Stepwise variation of actinic light intensity. 1. Experiment

RC photobleaching and absorption recovery kinetics after a stepwise variation in the cw actinic light intensity between two levels, I_1 and I_2, always reveals an easily detectable slow relaxation phase with the time constant greater than 10 s. See e.g., results in the previous section. The amplitude of this phase exceeds half of the total bleaching/recovery amplitude if the exposure time preceding the switching event is long enough (>10 s). Several representative traces of RC absorbance changes at 865 nm, the maximum of the primary photoelectron donor absorption band, under stepwise variation of the actinic light intensity between two different levels I_1 and I_2 are shown in Fig. 3. The measurements were

TABLE 1 Parameters of the model for RC samples prepared with different detergents

Detergent	Temp	x_P	x_B	k_P	k_B	α_P	α_B	γ_P	γ_B	k_{AP}	D_P	D_B
0.1% Na cholate	4°C	2	8	6	10	0.07	0.07	1.1	1.1	10	0.02	0.02
0.1% Na cholate	23°C	2	8	10	5	0.07	0.07	1.1	1.1	10	0.025	0.025
0.05% Triton X-100	23°C	2	8	10	5	0.07	0.07	1.1	1.1	10	0.025	0.025
0.05% LDAO	23°C	2	8	10	10	0.07	0.07	1.1	1.1	10	0.5	0.05

The uncertainties in the values of most fitting parameters are within ±15%. The diffusion constants D_P and D_B and the conformational coordinate value x_B are the most critical parameters and their values were estimated with an uncertainty of less than ±10%. The values $x_P = \Delta G_{AB}/k_BT = 2$ and $k_{AP} = 10$ were taken from the literature (see Kleinfeld et al., 1984; Goushcha et al., 2000).

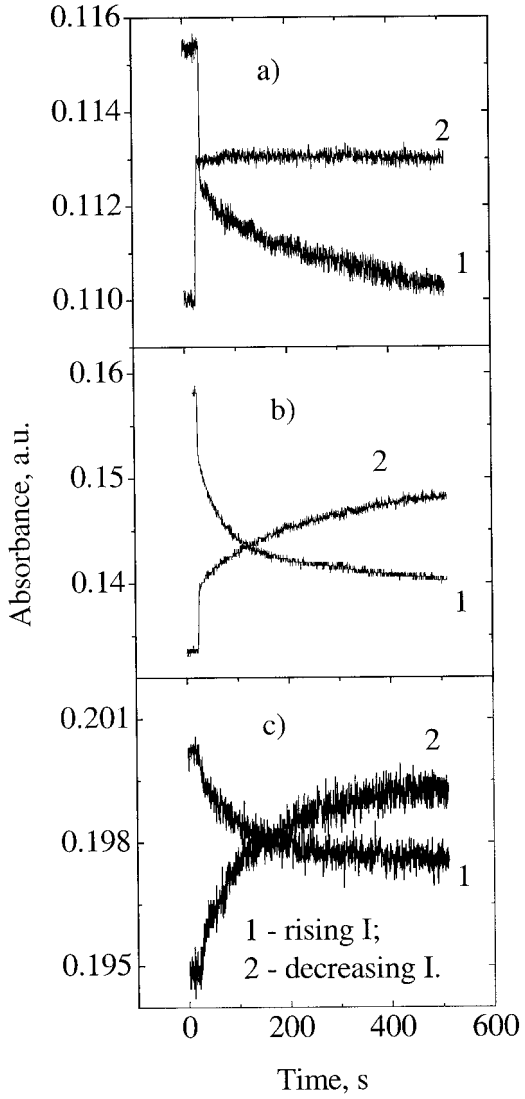

FIGURE 3 RC equilibration kinetics measured at 865 nm upon stepwise variation of the actinic light intensity between the levels 0.18 mW/cm^2 and 0.2 mW/cm^2 (*a*); 0.04 mW/cm^2 and 0.07 mW/cm^2 (*b*); 0.5 μW/cm^2 and 1.7 μW/cm^2 (*c*). $\lambda_{exc} = 850$ nm. Curves 1 and 2 in each graph correspond to light intensity increases and decreases, respectively. A steady-state absorbance was $A_{800} = 0.4$. Experimental conditions: 0.7 μM RC in the buffer 20mM Tris-HCl, pH 8.0, and 0.05% LDAO; ~80% of Q_B-active RCs and no quinone reconstitution procedure was applied; $T = 23$°C.

performed as follows. We started with the sample in the dark and applied a slow adiabatic increase of the cw actinic light intensity from $I = 0$ up to $I = 0.5$ μW/cm^2. Then the light intensity was rapidly increased to a slightly higher level, and the absorbance relaxation kinetics was measured. Following a waiting time to complete RC equilibration to a new quasiequilibrium level, the light intensity was again increased in a stepwise manner and the absorbance change was measured. Several more steps of a light intensity increase were applied until we reached the value of $I = 0.2$ mW/cm^2. This was followed by a stepwise decrease in I via the same set of the quasistationary state values.

When the values I_1 and I_2 were high enough ($I > 0.13$ mW/cm^2), the stepwise increase in I caused a sharp initial absorbance change (with a time constant ~1 s) followed by a slow relaxation with a half relaxation time of ~200 s (see e.g., *curve 1* in Fig. 3 *a*). On the other hand, the amplitude of any slow relaxation was negligible for a stepwise decrease of the actinic light intensity within the same interval although the fast initial change of absorbance was very pronounced (see *curve 2* in Fig. 3 *a*). Note that the final signal level of curve 2 never reaches the initial signal level of curve 1 on the timescale of the experiment. This result demonstrates a hysteretic behavior in RCs, indicating that thermally activated transitions over the potential maximum are nearly forbidden (see Discussion).

RC relaxation kinetics, measured with stepwise variation of I over an interval of intermediate light intensities (0.01 mW/cm^2–0.13 mW/cm^2), always exhibits comparable amplitudes of fast and slow relaxation phases (Fig. 3 *b*). Instantaneous variation of I over a very low light intensity interval (<1.7 μW/ cm^2) induces negligible amplitude of the fast relaxation component (with the time constant ~1 s) and a very pronounced slow phase (Fig. 3 *c*).

The total time of RC equilibration depended on both the light intensity switching interval and the final value I_2. An experimental demonstration for the case of a decreasing light intensity is shown in Fig. 4, in which the traces measured at various initial I_1 and final I_2 values of the actinic light intensity are normalized and superimposed. The fastest RC recovery kinetics with the slow phase half decay time of ~80 s was obtained when the final light intensity was rather high, $I_2 \geq 0.07$ mW/cm^2 (*curve 1* in Fig. 4). The equilibration kinetics slowed down when the final level I_2 was close to zero (*curve 2* in Fig. 4). The slow phase half decay time was ~140 s in this case. Finally, the slowest RC equilibration kinetics with $\tau_{1/2} \approx 250$ s was measured when I_2 value was between 0.001 mW/cm^2 and 0.07 mW/cm^2 (*curve 3* in Fig. 4).

Stepwise variation of actinic light intensity. 2. Modeling

Consider RC relaxation kinetics between two quasistationary states under abrupt, stepwise variation of actinic light intensity from I_1 to I_2. A stepwise change in the actinic light intensity causes the distribution function $P(t,x)$ to evolve in accordance with Eq. 3 at fixed $I = I_2$. If the adiabatic conditions mentioned above are fulfilled, the experimentally measured RC absorbance changes always reveal three pronounced components:

$$\Delta A(t) = \Delta A_{max} \cdot n_B(t) = \Delta A_{fast}(t) + \Delta A_{slow}(t) + \Delta A_{\infty},$$

the contributions of which to the total amplitude of a signal depend on both the system parameters and experimental conditions. The fast, purely electronic relaxation component is:

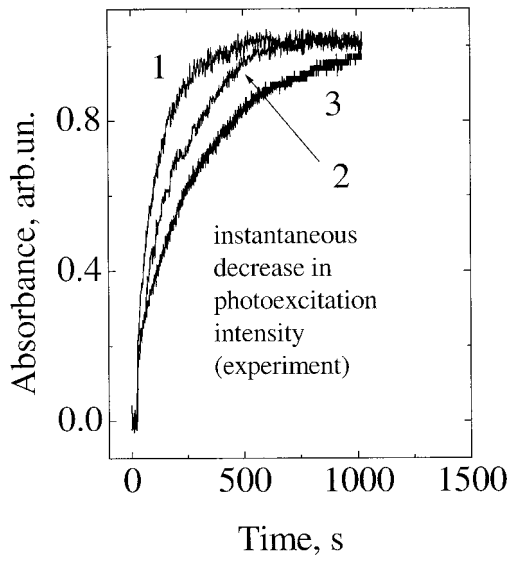

FIGURE 4 Experimentally observed RC equilibration kinetics measured at the maximum of the primary donor absorption band at $\lambda = 865$ nm and after a stepwise decrease of the actinic light intensity between different levels ($\lambda_{exc} = 850$ nm). Curve 1 was obtained for an I decrease between relatively high levels $I_1 = 0.13$ mW/cm^2 and $I_2 = 0.07$ mW/cm^2. A stepwise decrease of I down to the intermediate light intensity level produced a very slow equilibration kinetics, which is shown by curve 3 ($I_1 = 40$ μW/cm^2 and $I_2 = 14$ μW/cm^2). The intermediate rate of relaxation kinetics was measured after stepwise decrease of I from $I_1 = 4$ μW/cm^2 to $I_2 = 0$ (*curve 2*). The sample: *Rb. sphaeroides* RCs isolated with 0.05% LDAO. The buffer conditions are the same as in Fig. 2. $T = 23$°C.

$$\Delta A_{fast}(t) = \Delta A_{max} \cdot \int dx \frac{\exp\left(-\frac{V^{eff}_{I_1}(x)}{k_B T}\right)}{z(I_1)} \left[\frac{I_1}{I_1 + k_{AP} \cdot e^{-x}} - \frac{I_2}{I_2 + k_{AP} \cdot e^{-x}}\right] \cdot \exp[-(I_1 + k_{AP} \cdot e^{-x}) \cdot t]. \quad (6)$$

The second, slow kinetic phase

$$\Delta A_{slow}(t) = \Delta A_{max} \cdot \int dx \left[P(t, I_2) - \frac{\exp\left(-\frac{V^{eff}_{I_2}(x)}{k_B T}\right)}{z(I_2)}\right] \times \frac{I_2}{I_2 + k_{AP} \cdot e^{-x}} \quad (7)$$

corresponds to adiabatic changes in electronic populations of the cofactors, which proceed concomitantly with the structural diffusion toward a new equilibrium. See Barabash et al., 2002, for more details. Finally,

$$\Delta A_{\infty} = \Delta A_{max} \cdot \int dx \frac{\exp\left(-\frac{V^{eff}_{I_2}(x)}{k_B T}\right)}{z(I_2)} \cdot \frac{I_2}{I_2 + k_{AP} \cdot e^{-x}} \quad (8)$$

is a new stationary absorbance value that corresponds to the photoexcitation intensity I_2.

Fig. 5, *a–c*, shows adiabatic potentials at three pairs of levels of the initial I_1 and final I_2 light intensity, $V^{eff}_{I_1}(x)$ and $V^{eff}_{I_2}(x)$. Note that because the light intensity varied only slightly, the difference between $V^{eff}_{I_1}(x)$ and $V^{eff}_{I_2}(x)$ is barely seen on the graphs. The corresponding kinetics of photoexcitation and recombination are shown to the right in Fig. 5, *d–f*. In each computational run of the photoexcitation kinetics, the excitation intensity was switched from 0 to I_1 and was held unchanged during 5000 s until complete equilibration of the system. Then the excitation intensity was increased instantaneously to I_2 followed by another 5000 s of equilibration time. The initial 1500-s time intervals are shown in Fig. 5, *d–f*. In calculating the recombination kinetics, the excitation intensity was first increased from 0 to $I = 2$ s^{-1}, followed by instantaneous switching down to $I_1 > I_2$ and then further down to I_2. Note that stationary-state absorption levels, which correspond to the same excitation levels, were always identical for increasing and decreasing excitation intensity. This was not the case for the experimental observations in Fig. 3. The reason for this divergence comes out of the limitations of the model, and will be discussed below. We used s^{-1} for the excitation intensity units. For *Rb. sphaeroides* RCs, the excitation level of 1 s^{-1} corresponds to an actinic light intensity of 0.4 ~ 1.4 mW/cm^2

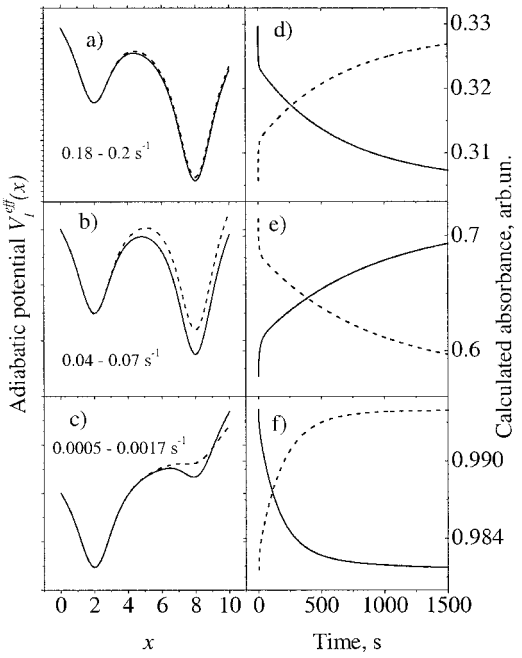

FIGURE 5 Adiabatic potential changes induced by an instantaneous variation in photoexcitation intensity (graphs *a–c*). The low-intensity potential surfaces are shown with dashed lines. The curves to the right of each potential show RC equilibration kinetics calculated for the cases of increasing (*dashed lines*) and decreasing (*solid lines*) excitation intensity (see graphs *d–f*). The variation of excitation intensity produced very small changes in the adiabatic potential; therefore the potential surfaces corresponding to the two different values of I (these values are indicated on the graphs) are hardly distinguishable on each graph.

at 865 nm (Manzo et al., unpublished). In this paper, we set 1 s^{-1} as equal to 1 mW/cm^2.

The results of modeling show that upon changing the excitation light intensity, the excess population slowly equilibrates from one potential valley over the potential maximum to the other valley. The characteristic time of this process obviously depends on the barrier height and determines the character of the slow equilibration kinetics for both photoexcitation (bleaching) and recombination. More detailed consideration shows that this characteristic time is determined by the depth of the shallower potential valley, and we will refer to this particular time in the following discussion.

Fig. 6 shows the results of modeling, analogous to the experimental results presented in Fig. 4. To facilitate observation, the photoexcitation intervals were selected to be further apart from each other than were the corresponding experimental intervals in Fig. 4. The half decay time of the slow kinetic phase was ~180 s for switching the excitation intensity between the levels $I_1 = 5.0\ s^{-1}$ and $I_2 = 4.0\ s^{-1}$ (*trace 1* in Fig. 6). Switching of I between $I_1 = 0.004\ s^{-1}$ and $I_2 = 0.0001$ produced considerably slower relaxation kinetics with the half decay time of the slow phase $\tau_{1/2} \approx 250$ s (*trace 2* in Fig. 6). The slowest relaxation kinetics ($\tau_{1/2} \approx$ 340 s) was calculated for the case $I_1 = 0.1\ s^{-1}$ and $I_2 = 0.05\ s^{-1}$ (*trace 3* in Fig. 6). The value of a slow phase decay time was only slightly dependent on the initial level of photoexcitation intensity I_1, whereas the variation in the final value I_2 caused considerable changes in overall relaxation kinetics.

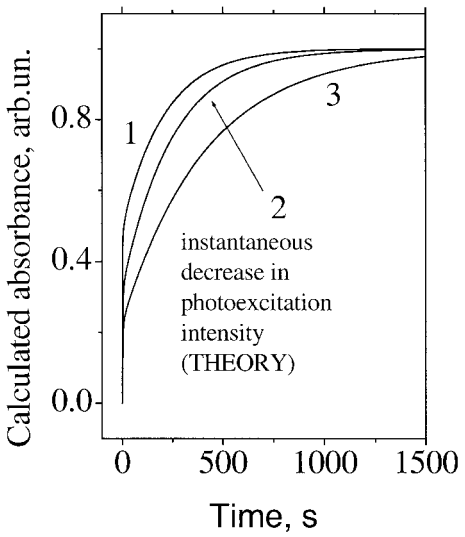

FIGURE 6 Calculated RC equilibration kinetics after an abrupt photoexcitation decrease between two quasistationary-state levels: from $I_1 = 5.0\ s^{-1}$ to $I_2 = 4.0\ s^{-1}$ (*curve 1*); from $I_1 = 0.004\ s^{-1}$ to $I_2 = 0.0001\ s^{-1}$ (*curve 2*); and from $I_1 = 0.1\ s^{-1}$ to $I_2 = 0.05\ s^{-1}$ (*curve 3*). The curves are normalized to unity and superimposed. The model parameters were the following: $x_P = 2$; $x_B = 8$; $k_P = 10$; $k_B = 10$; $\alpha_P = \alpha_B = 0.07$; $\gamma_P = \gamma_B = 1.1$; $D_P = 0.5\ s^{-1}$; $D_B = 0.05\ s^{-1}$; and $k_{AP} = 10\ s^{-1}$.

Actinic pulses applied to a preilluminated sample. 1. Experiment

Some of the results presented in this section were described briefly in our recent paper (Barabash et al., 2002). Here we present more experimental evidence and some important details that have not been discussed previously.

Nonequilibrium dynamic effects occurring due to accumulation of structural changes after multiple, consecutive turnovers of RCs can be revealed in the following straightforward experiment. RCs were illuminated with cw actinic light of close to saturation intensity ($P_{cw} = 1$ mW/cm^2, $\lambda_{exc} = 835$ nm). After cessation of the cw photoexcitation, the sample was illuminated with a sequence of short actinic pulses spaced at a variable time interval (peak intensity $P_{flash} = 1$ mW/cm^2, $\lambda_{flash} = 835$ nm). Fig. 7 summarizes results obtained in experiments with RCs containing three different detergents. The exposure time was 200 s, the duration of each pulse in a sequence was 0.4 s, the first pulse was triggered 5 s after cessation of the cw illumination, and the pulses spacing time was 250 s. The reference curves measured in analogous experiments but with actinic pulses blocked are also shown in each graph. The slow relaxation phase with a time constant >10 s, which was not observed in a single flash activated kinetics applied to a dark-adapted sample (not presented in this paper), was normally detected after each pulse in a sequence. The amplitude of this phase was the biggest for RCs with Triton X-100 (*graph b* in Fig. 7). RCs with Na cholate also showed an easily observed slow relaxation phase after each flash (*graph c* in Fig. 7), whereas the amplitude of this phase for RCs with LDAO was relatively small (*graph a* in Fig. 7). The amplitude of the slow relaxation phase was negligibly small after the first flash in a sequence for each sample. This is clearly seen in Fig. 8, in which the difference between the traces measured with actinic pulses and reference traces is shown. The amplitude of a slow relaxation phase was the highest a few minutes after cessation of cw illumination, and it diminished considerably by the end of the experiment.

Fig. 9 shows normalized and superimposed traces of the pulses from each graph of Fig. 7. The traces coincide precisely with each other except for the one after the first pulse in a train. This deviation of the first trace is due to a steep slope of the relaxation curve at the instant of the first pulse triggering. Subtracting this slope from the signal provides an exact coincidence of the first trace with other ones (not shown in the Fig. 9). It means that for any investigated sample, the fast phase of relaxation with contributions of 0.1 s and 1 s components was identical after each pulse in a train. This important experimental result mirrors an equivalent result in the theoretical studies described in the following section.

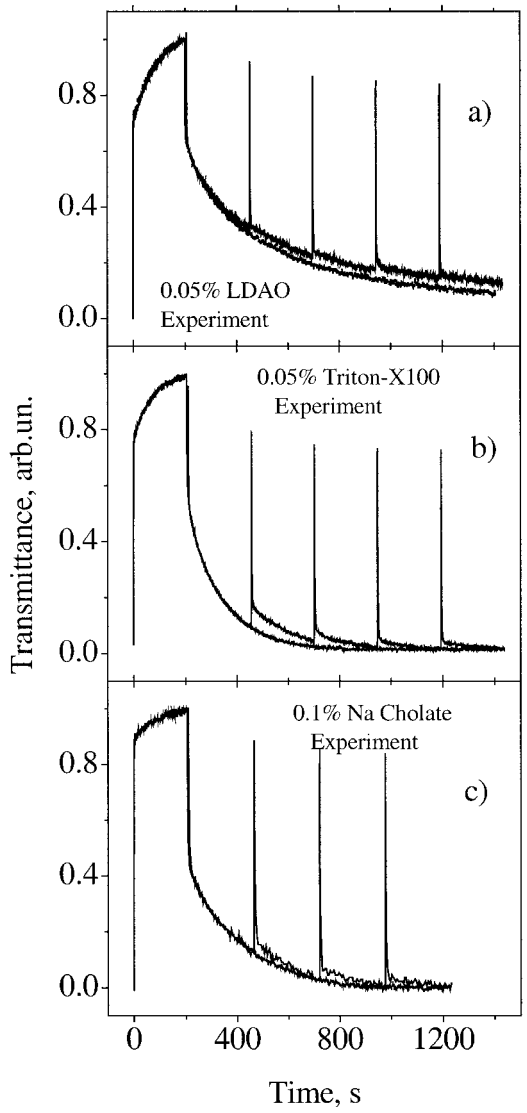

FIGURE 7 RC transmittance changes (at 835 nm) after a stepwise variation of actinic light intensity. The cw actinic light ($I = 1$ mW/cm^2, $\lambda_{exc} =$ 835 nm) was turned on at the instant $t = 5$ s and was off at $t = 205$ s. A train of actinic flashes spaced at 250 s time intervals was applied 5 s after turning off a cw actinic light. Transmittance changes after the first flash are not resolved on the graphs. The reference signals measured in separate runs with actinic flashes blocked are also shown on the graphs.

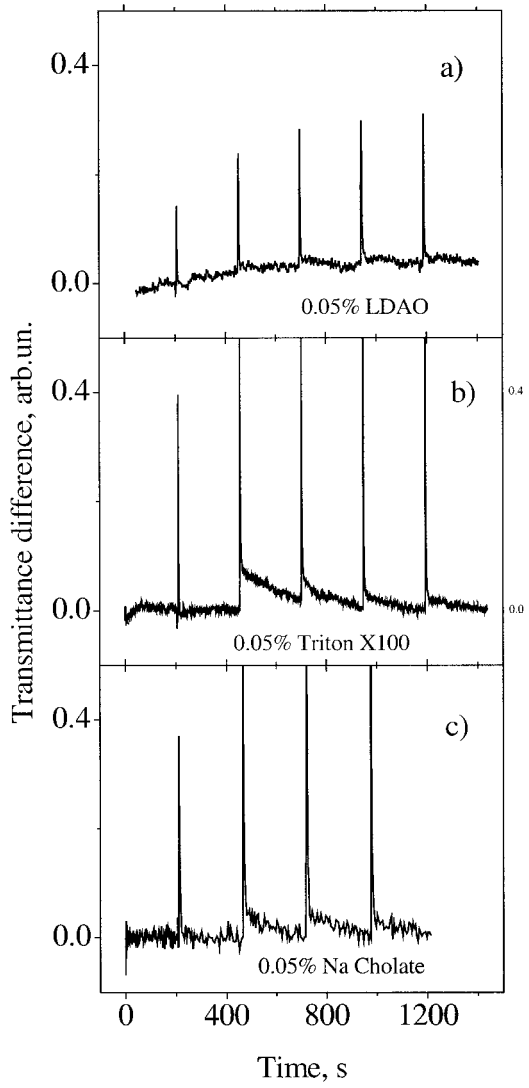

FIGURE 8 The difference between the traces recorded with applied actinic flashes and reference traces. Note the absence of the slow relaxation component after the first pulse on each graph.

Actinic pulses applied to preilluminated sample. 2. Modeling

Let us consider RC transmittance upon stepwise increase of photoexcitation intensity from $I = 0$ to a certain maximum level I_{max} followed by a 200-s exposure time and subsequent switching off the photoexcitation. The computer analysis in accord with Eqs. 1–3 and using a specific set of parameters for each sample as determined above was made employing two different protocols. In one run, an additional pulsed photoexcitation of the system was generated with a train of high-intensity ($I = 1$ s^{-1}), 0.4-s duration pulses. The instant of the first pulse generation and the time spacing between the pulses in a train were the same as in corresponding experimental studies (see the previous section). In the other run, no pulsed excitation has been generated and the reference trace was computed.

Fig. 10 shows the results of computer simulations for RCs with LDAO (*graph a*) and for those with either Na cholate or Triton X-100 (*graph b*). The amplitude of a slow relaxation phase (with the time constant >200 s) was significant for the set of parameters characteristic for RCs with either Na cholate or for those with Triton X-100 after the second and several subsequent pulses. See graph *a* in Fig. 11, in which the difference between the two traces of each graph in Fig. 10 is presented. For the case of RCs with LDAO, only a slightly noticeable ''accumulation'' of the slow relaxation component was obtained after each pulse in a train (*graph b* in

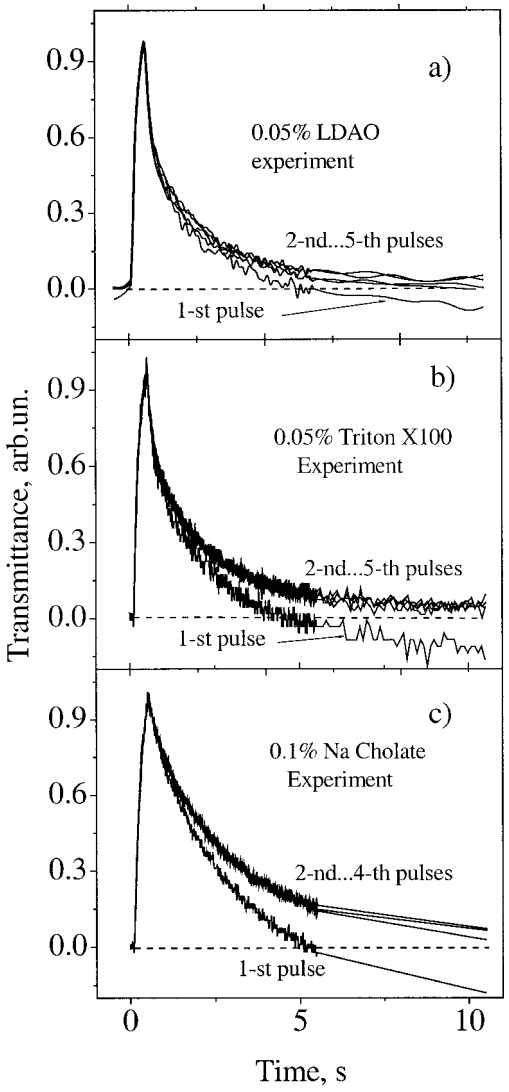

FIGURE 9 Comparison of RC response to each of the actinic flashes in a train. The 10-s duration traces were cut from the corresponding curves in Fig. 5, then normalized to unity and superimposed.

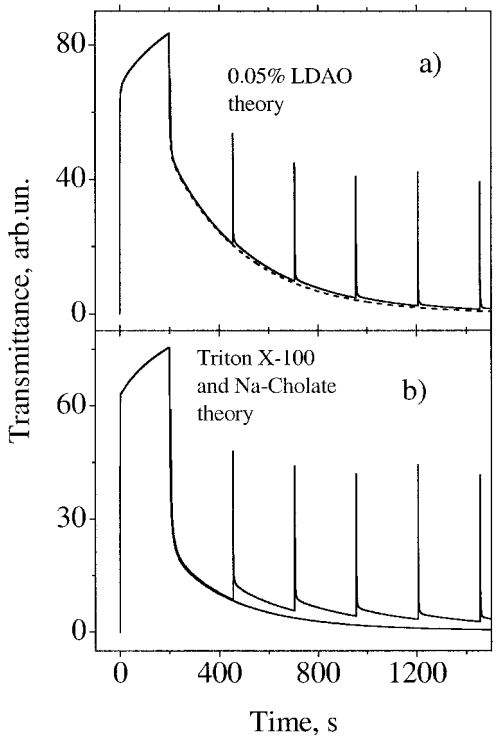

FIGURE 10 Results of modeling of RC response to 200-s duration cw actinic light followed by photoexcitation with a sequence of pulses. Each graph shows also a result of a separate run without generating photoexciting pulses (a reference trace). The first pulse in a sequence (not resolved on the graphs) was generated 5 s after cessation of cw photoexcitation. The parameters of the model for the traces on the graph (*a*) were as follows: $x_P = 2$; $x_B = 8$; $k_P = 10$; $k_B = 10$; $\alpha_P = \alpha_B = 0.07$; $\gamma_P = \gamma_B = 1.1$; $D_P = 0.5$ s^{-1}; $D_B = 0.05$ s^{-1}; and $k_{AP} = 10$ s^{-1}. The traces on the graph (*b*) were obtained for the same set of parameters as above except of $k_B = 5$; $D_P = D_B = 0.025$ s^{-1}.

Fig. 11). The amplitude of a slow relaxation component after the first pulse was always negligibly small for each system.

The details of each system reaction to every generated pulse in a train are presented in Fig. 12, where the corresponding, 10-s duration parts of the curves in Fig. 10 are cut, normalized, and superimposed. No essential difference between kinetic traces in a sequence was obtained except for the very first pulse, but this effect is due to a steep slope of the background relaxation at the instant of the first pulse generation. This finding is in complete agreement with experimental results. Compare with Fig. 9. The accumulation of structural changes after consecutive turnovers of RCs (structural memory effect) that drives the system toward a ''light'' conformational state does not influence the fast phase (0.1 s and 1 s components) of the system response to a single actinic pulse applied at any time after turning off cw photoexcitation of a system. In contrast, the system response to a single pulse on a long timescale (>10 s) depends strongly on both the pulse number in a sequence and the dynamic properties (diffusion constants and elastic constants) of a system.

DISCUSSION

The features of RC equilibration kinetics described above cannot be accounted for by the effects of charge capture by nonfunctional traps, by branching of the electron transfer reaction in the early stages of charge separation, or by reversible denaturation of RCs during their prolonged illumination with high-intensity actinic light. A pronounced dependence of relaxation kinetics on the interval of light intensity switching is not a conventional characteristic of a simple, open physical system. In contrast, the nonlinear dynamic properties arising due to a strong charge-conformational interaction is the most probable candidate to account for the effects observed. When either the final light intensity value I_2 or both the initial I_1 and final I_2 values fall

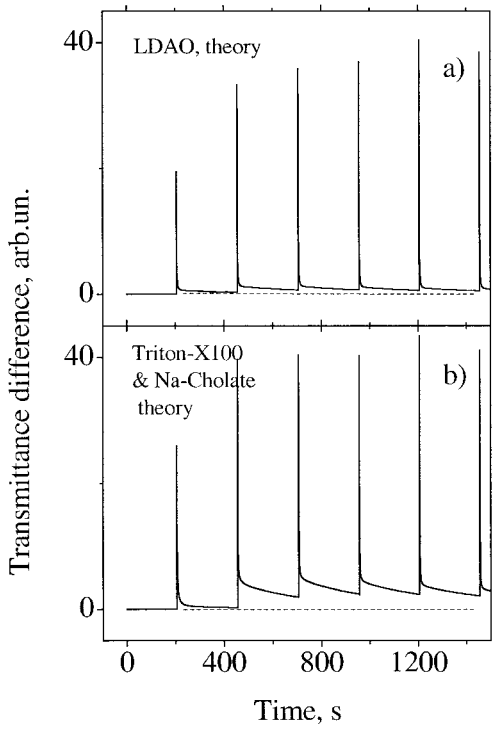

FIGURE 11 The difference between traces calculated with photoexciting pulses on and reference traces. Note the absence of the slow relaxation component after the first pulse on each graph (compare with corresponding experimental graphs in Fig. 6).

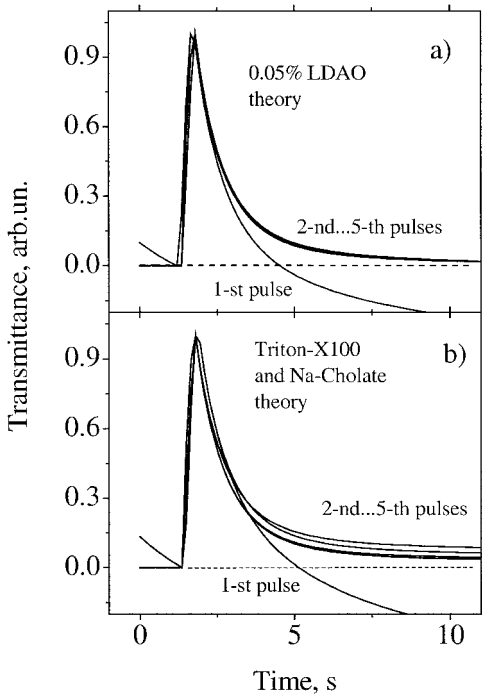

FIGURE 12 Comparison of pulses in sequences shown in Fig. 8. The 10-s duration traces were cut from the corresponding curves in Fig. 8, normalized to unity, and superimposed. The initial five pulses for each system are shown.

within the bistability domain, the adiabatic potential that describes RCs under these nonequilibrium conditions is not a simple single well potential (Goushcha et al., 2000), and very interesting, nontrivial equilibration kinetics like those described above may be observed.

Qualitatively let us consider the charge separation process upon continuous photoactivation at intensity I. Initially, at the instant of switching on a continuous actinic light, all RCs are in a state with the electron localized on the donor and with the value of the structural variable x close to the dark value x_P. After the actinic light is switched on, charge separation proceeds and the quasistationary state distribution of RCs over the states with the electron localized either on the donor or on the acceptor is reached after the characteristic time interval $\tau_{el} = (I + k_{AP}e^{-x_P})^{-1}$:

$$\frac{\rho_B^{st}(x, I)}{\rho_P^{st}(x, I)} = \frac{I}{k_{AP}e^{-x_P}} = \frac{I}{k_{AP}}e^{x_P}. \quad (9)$$

RCs with separated charges gradually begin to undergo conformational changes (on the time scale $\gg \tau_{el}$) that can be modeled as movement (diffusion) of the RC distribution along the upper potential surface (see Fig. 13) toward its minimum x_B, corresponding to the light-adapted conformational state.

Assuming that during the time interval Δt the charge recombination in the selected reaction center has not yet occurred, the value of the generalized conformational coordinate in this RC will increase by the amount Δx and reach a value of $x = x_P + \Delta x$. This causes a decrease in the recombination rate constant to $k_{AP}e^{-(x_P+\Delta x)}$, whereas the photoexcitation intensity does not change. The balance between RC population with the electron on the donor and that with separated charges is shifted toward the latter state, i.e.:

$$\frac{\rho_B^{st}(x, I)}{\rho_P^{st}(x, I)} = \frac{I}{k_{AP}e^{-(x_P+\Delta x)}} = \left(\frac{I}{k_{AP}}e^{x_P}\right)e^{\Delta x}. \quad (10)$$

Such an increase of the portion of RCs with separated charges corresponds to the slow phase of bleaching kinetics in Fig. 2 because these phase kinetics are determined by the rate of RC conformational change at a constant photoexcitation intensity. See also the slow (structural) relaxation phase in the charge separated state, Fig. 13. However, at ''low'' photoexcitation intensity, the RC, after charge recombination, has enough time to return back to the minimum x_P of the dark (charge-neutral) potential. This sequence of electronic transitions and structural rearrangements corresponds to cycle 1 in Fig. 13. Therefore, under ''low'' actinic light intensity, the RC will accumulate only a slight conformational change with a coordinate x that is close to the dark-adapted value of the structural variable x_P.

At high photoactivation intensities, a slight conformational change during the first charge separation event of the RC does not have enough time before the next charge

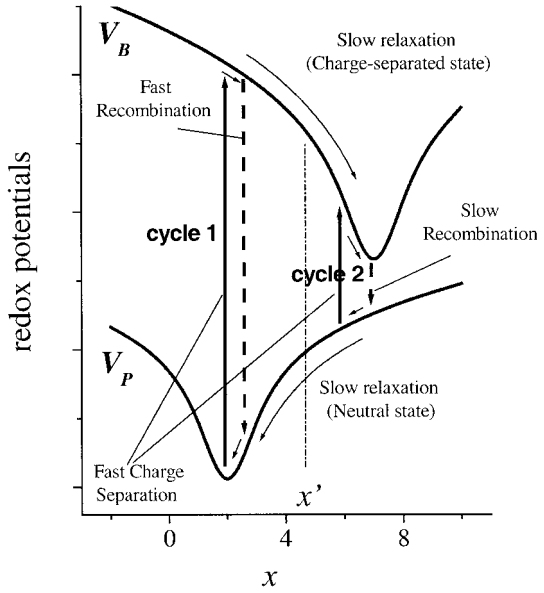

FIGURE 13 Simplified qualitative description of electronic and conformational transitions during the charge separation and recombination in RC. The lower potential surface represents the redox potential of the charge-neutral state, whereas the upper potential describes the charge-separated state. The fast charge-separation (bleaching) phase corresponds to electronic transitions ''up'' at different but fixed values of the structural variable x. The fast recombination phase appears due to electronic transitions ''down'' (charge recombination) around $x = 2$ only. The slow phase of structural relaxation in the charge-separated state appears due to the bounded diffusion along the upper potential surface to the right and causes the slow photobleaching phase in Fig. 2. The slow recombination phase arises due to both the charge recombination in the highly deformed state (around $x = 8$) and electron-conformational transitions governed by the diffusion/drift along the potential surfaces to the left. See text for more details.

separation event to fully relax back along the lower potential surface (the slow (structural) relaxation phase in the charge-neutral state, Fig. 13) to the initial, dark-adapted state ($x \approx x_P$). The next photoactivation of the RC and following charge separation occurs with the macromolecule already in a slightly changed conformational state. This ratcheting of the conformation is a key feature of the model because the effects of accumulated structural changes and self-regulation could only become possible under the condition of noticeable structural memory in the system (see also Barabash et al., 2002). The ratcheting process repeats after each charge recombination event and the conformational change increases. As a result, under continuous wave photoexcitation, the RC gradually undergoes conformational change until it attains the minimum of the potential surface of the light adapted state x_B. A high photoexcitation frequency does not allow the RC to fully return to the point $x = x_P$, and the RC conformational coordinate now fluctuates around the structural variable value x_B. See cycle 2 in Fig. 13.

The most interesting effects occur at intermediate light intensities. In this case, cycle 1 and cycle 2 may coexist. I.e., if the initial conformational change of the RC was relatively slight, the system fluctuates according to cycle 1; if, alternatively, the initial change was larger than some specific value x', then the system behavior is described by cycle 2. This effect is related to the charge recombination rate dependence on the structural variable value. This qualitative analysis of kinetics of electronic transitions and associated conformational changes in RCs is rigorously described by the nonequilibrium effective adiabatic potential $V_I^{\text{eff}}(x)$, which was defined in Eq. 2 (see Goushcha et al., 2000, part 1; Christophorov, et al., 2000). The second term in Eq. 2 accounts for the force that causes the conformational change in an RC with separated charges. This term depends on both the curvature of the potential surface of RC in the charge-separated state and the survival time in this state. The latter is determined by the relationship between the rate constants of photoexcitation and recombination, to be precise by the value $\rho_B^{st} = I/(I + k_{AP}e^{-x})$. The form of the first term in Eq. 2 is analogous to that of the second term, and it determines the force acting on the structural variable after the charge recombination is complete. This force drives the structure back toward the dark-adapted state (the dark value of the structural variable). As shown in Fig. 14, the effective potential has a single minimum at either $x = x_P$ at low photoexcitation intensities or $x = x_B$ at high photoexcitation levels. At intermediate levels of cw actinic light, the structural variable effective potential has two minima and exhibits properties of a photoinduced bistability. The potential maximum corresponds to the critical deformation x' that divides the two structural states, and the depths of potential minima depend on the actinic light intensity. This is a remarkable property of the effective potential that allows its application for the description of RC thermodynamic properties in light-induced structural transitions.

The recombination process rate depends on an extent of the structural variable deformation and can vary continually.

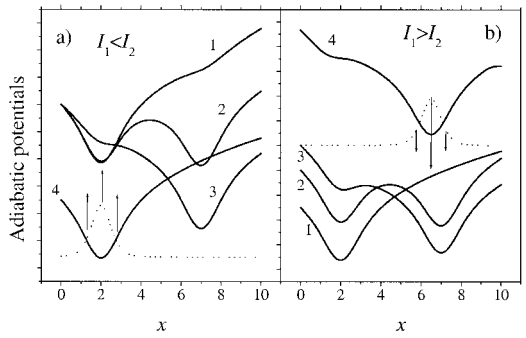

FIGURE 14 Possible cases for the effective potential shape change at various light intensities (graph *a*—increasing light intensity *I*, graph *b*—decreasing *I*). The initial state is represented with potential curve 4 on each graph. Three possible cases of the final state are represented with the potential surfaces 1 (low excitation intensity), 2 (medium excitation intensity), and 3 (high excitation intensity). The dotted line shows the distribution function at the initial excitation intensity and arrows indicate schematically the direction of electronic transitions.

A pronounced biphasicity in the recombination curve provides evidence that the recombination kinetics is determined mainly by either almost nondeformed (fast recombination phase) or heavily deformed RCs (slow recombination phase), reflecting thereby the bistable nature of the adiabatic conformational potential. Note that the slow recombination phase has also a minor contribution from the combined electron-conformational transitions, in which a decrease/increase of the structural deformation precedes the electron recombination itself.

Practically any process of RC photoexcitation or recombination, except maybe in the case of charge recombination in an experiment when lengthy and intensive actinic illumination to a sample is turned off completely, can be effectively described using the formalism of a nonequilibrium adiabatic potential. In other words, this formalism is applied if, at a final light intensity I_2, the value $\tau_{el}(x, I_2) = (I_2 + k_{AP}e^{-x})^{-1}$ remains small enough for the adiabatic approximation to hold true.

Under continuous photoexcitation and applying adiabatic elimination of the fast electronic transitions, i.e., by reduction of Eq. 1 to Eq. 3, the redox potentials V_P, V_B are not suitable for describing the structural state of the RC. Conversely, the nonequilibrium effective adiabatic potential $V_I^{eff}(x)$ gives an adequate description. The shape of $V_I^{eff}(x)$ depends both on the redox potentials V_P, V_B and on the photoactivation intensity, I. Note that the initial redox potentials V_P, V_B were chosen as single valley potentials (see Fig. 13 and Eq. 4). Conversely, the effective potential $V_I^{eff}(x)$ has two minima within the bistability domain (i.e., over a specific interval of I only) independently of the location of the electron. Due to fast electron transitions, in the adiabatic approximation, the structure senses only the time-averaged electron density.

Fig. 14 describes qualitatively three possible characteristic cases of the shape of the effective potential. Corresponding changes in the distribution function $P(x, t)$ over the structural variable are described by Eq. 3 and can be revealed in slow components of the equilibration kinetics when diffusion along the structural variable proceeds while overcoming a noticeable barrier of $V_I^{eff}(x)$. For the case of photoexcitation (bleaching), we chose $I_1 = 0$, whereas the three different I_2 levels were chosen in the way that the corresponding adiabatic potentials describe three possible cases:

1. Low excitation intensity. Charge photoseparation leads to a weak structural deformation, which is not strong enough for bistability to occur. The adiabatic potential has only one, ''dark'' minimum. The second, ''light'' minimum does not appear. See curve 1 in Fig. 14 *a*. The equilibration kinetics will not exhibit a very slow equilibration component.
2. Medium excitation intensity. The excitation intensity is strong enough for the bistability to occur. The depths of the ''dark'' and ''light'' conformational valleys are approximately equal (*curve 2* in Fig. 14 *a*) and the probabilities for each of the two possible conformational states are approximately equal. The equilibration (bleaching) kinetics will be biphasic with comparable amplitudes of both phases. The relaxation time constant of the slow equilibration component will be much longer than in case 1).
3. High excitation intensity. Photoexcitation leads to strong light-induced structural changes resulting in disappearance of the ''dark'' conformational state and creation of the ''light'' conformational state. The adiabatic potential is again monostable, although a slightly pronounced shoulder around small values of x evidences the influence of the potential of the charge-neutral redox state (*curve 3* in Fig. 14 *a*). The photoexcitation (bleaching) equilibration kinetics will be generally biphasic but the slow phase will not be as grossly delayed as in case 2).

For the recombination process, the schematic representation of the initial and final adiabatic potentials is reversed with respect to the case of photoexcitation (bleaching). See Fig. 14 *b*. The initial excitation intensity I_1 was chosen to be high enough to produce a monostable adiabatic potential with the ''light'' conformational state only. The three final values I_2 were chosen in the way that corresponding adiabatic potentials described three possible cases like we made above for the case of photoexcitation (bleaching). The recombination equilibration kinetics in any of the three cases is generally biphasic. The equilibration time should be expected to be the slowest for the case of intermediate values of I_2.

The above features of RCs equilibration kinetics were observed experimentally (Figs. 3 and 4) and modeled theoretically (Figs. 5 and 6). In the case of the lowest light intensities I_1 and I_2, when the potential barrier that separates the two stable states is either relatively low or completely vanishes (see e.g., Fig. 5 *a*), the time constant of the slow component of equilibration kinetics is ~200 s or smaller. See experimental results in Fig. 3 *c* and curve 2 in Fig. 4 and corresponding results of modeling in Fig. 5 *d* and curve 2, Fig. 6. The amplitude of the fast equilibration component is very small in this case mainly due to the small factor $[I_1/(I_1 + k_{AP} \cdot e^{-x}) - I_2/(I_2 + k_{AP} \cdot e^{-x})]$ in the expression for the fast relaxation component (see Eq. 6). Upon increasing the light intensities I_1 and I_2, the amplitude of the fast relaxation component increases monotonically. At intermediate light intensities, when the depths of potential minimums are almost equal, the potential maximum reaches its maximum height (see e.g., Fig. 5 *b*) and the time constant of the slow equilibration component becomes very long (300 s or longer). See experimental results in Fig. 3 *b* and curve 3 in Fig. 4 and corresponding results of modeling in Fig. 5 *e* and curve 3, Fig. 6. A further increase in the photoexcitation intensities I_1 and I_2 leads to a decrease of the potential barrier height (see Fig. 5 *c*) that results in corresponding acceleration of the equilibration kinetics. See experimental results in Fig.

3 *a* and curve 1 in Fig. 4 and corresponding results of modeling in Fig. 5 *f* and curve 1, Fig. 6.

A pronounced asymmetry in the slow equilibration phases of photoexcitation (bleaching) and relaxation process essentially distinguishes experimentally measured kinetics (Fig. 3) from the calculated dependencies (Fig. 5). One possible reason for this difference could be a significant obstacle to the thermally assisted transitions over the potential barrier due to roughness in the potential surface, which has not been taken into account in calculations (Frauenfelder et al., 1991). Experimentally, this phenomenon results in a significant delay in equilibration of the true stationary state at a particular light intensity within the bistability domain. As a result, the measured absorbance can be slightly lower than the true stationary-state value for the increasing excitation intensity, whereas this value for the case of a decreasing excitation intensity can be higher than the real stationary-state value. Unfortunately, it is usually very difficult to detect a true stationary state in a real experiment. Note that accounting for such effects could only slightly modify the modeling results obtained here (see e.g., Fig. 5), making them closer to the experimentally measured kinetic dependences (Fig. 3).

Note also that an asymmetry of RC photoexcitation (bleaching) and recombination kinetics is an inherent property that could be observed any time the exciting light intensity is switched between two quite different levels. For example, if one light intensity level is very high and a corresponding adiabatic conformational potential has a single, ''light'' valley and the other light intensity level corresponds to the adiabatic potential with the two approximately equal valleys, then the instantaneous decrease in the actinic light intensity between these two levels will cause a very long equilibration phase. In contrast, the disappearance of the barrier upon rapidly increasing light intensity up will result in a very fast equilibration of the system (see Fig. 15).

Now we consider our results on the effect of a train of photoexcitation flashes applied to the preilluminated sample on RC relaxation kinetics. Consider first results for RCs either with 0.05% Triton X-100 or with 0.1% Na cholate. The slow relaxation component, which was completely absent in the primary donor recovery kinetics after a flash applied to the dark-adapted samples, appeared in relaxation kinetics after the second and several subsequent pulses in preilluminated samples. We consider this result to be a clear evidence for long-lived structural changes induced by photoseparated charges in RCs during their lengthy preillumination. Note that the slow relaxation component is always negligibly small in the kinetic traces measured after the first flash in a train (see Fig. 8). The explanation for this observation is straightforward. The time interval of 5 s between the cessation of cw actinic light and instant of the first flash is a very short time to accumulate any noticeable amount of RCs with a highly deformed structure (large values of $x \sim x_B = 8$) in the electronically ground

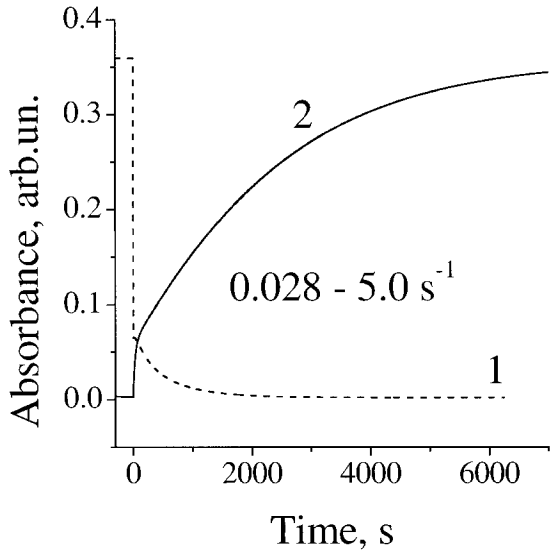

FIGURE 15 RC photoexcitation (bleaching) (*dashed curve 1*) and recombination (*solid curve 2*) kinetics calculated using Eq. 5 for the excitation switching ''up'' and ''down'' between the levels 0.028 s^{-1} and 5.0 s^{-1}. The parameters of the model were as follows: $x_P = 2$; $x_B = 8$; $k_P = 10$; $k_B = 10$; $\alpha_P = \alpha_B = 0.07$; $\gamma_P = \gamma_B = 1.1$; $D_P = 0.5\ s^{-1}$; $D_B = 0.05\ s^{-1}$; and $k_{AP} = 10\ s^{-1}$.

state. Recall that the recombination time constant for photoexcited RCs with highly deformed structure is $\tau_{rec}(x) = k_{AD}^{-1}\exp(x_B) \approx 300\,s$.

At the instant of the second flash, a significant amount of RCs with the deformed structure has accumulated in the ground state, producing a pronounced retardation of relaxation after a flash. The third, fourth, and fifth flashes also result in significant amplitudes of the slow relaxation phase, although these amplitudes decrease gradually with flash number (see *graphs b* and *c* in Fig. 8). Such a dependence of the amplitude of the slow relaxation phase is determined by the competition between the charge recombination process that enriched the population of the ''light'' conformational state with charge-neutral molecules, and diffusion/drift of this pool of population toward the equilibrium in the ''dark'' potential valley. The latter process defines the diffusion constant D_P and controls the relaxation time of the structure to a dark-adapted state. See Fig. 13, a slow (structural) relaxation phase in the charge-neutral redox state. Obviously this competition is advantageous for RC accumulation in the electronically ground state with a deformed structure in the case of the samples with 0.05% Triton X-100 or with 0.1% Na cholate.

For the samples with 0.05% LDAO, the competition favors rapid depletion of the ''light'' conformational state of RCs with the deformed structure. The diffusion constant D_P for these samples was large enough to ensure a low population of the ''light'' conformational valley with charge-neutral RCs before each flash in a train. Note that such a low efficiency of accumulation of charge-neutral, structurally deformed RCs is still sufficient to drive the major portion of

RCs toward the ''light'' conformational state upon lengthy illumination of the sample with high-intensity actinic light. In other words, multiple turnovers of RCs under the condition when each RC is photoexcited immediately after charge recombination occurred efficiently drives the whole pool of RCs toward its equilibrium in the ''light'' conformational valley. Cessation of cw actinic illumination in this case results in recovery kinetics with a large amplitude slow relaxation for all samples (see Fig. 7).

The slow relaxation component, with a time constant $\gg$10 s, has not been observed in the flash-activated kinetics of thoroughly dark-adapted samples with any of the three different detergents used in this work. The initial part of the primary donor recovery kinetics after a flash applied to a preilluminated sample does not depend on the delay time between cessation of cw photoexcitation and the flash instant for any of the three samples (see Fig. 9 and Fig. 12). This observation is the same as that reported for RCs isolated with 0.025% LDAO in the recent work by F. van Mourik with coworkers (van Mourik et al., 2001). This result alone does not allow for the conclusion made in the cited work that the structural memory effects, which induce nonlinear dynamic behavior of RCs, did not influence their function. In contrast, computer modeling based on nonlinear dynamic theories made in the present work shows that the initial stage of RC relaxation kinetics after a flash must be the same for each flash in a train of pulses applied to a preilluminated sample (see Fig. 10). In contrast, the equilibration kinetics in the late stage of RC relaxation ($\gg$10 s) after each flash in a train may (or may not) be different from the flash activated kinetics measured in the dark-adapted sample. The realization of one of the two mentioned alternatives depends on the trade-off between the diffusion time along the ground state potential surface (which is determined by D_P) and the survival time of the charge separated state.

Results on RC equilibration kinetics described in this work were essentially the same for the samples obtained from two different research groups. The effects of different detergents on the protein nonequilibrium dynamic properties may be readily attributed to the influence of the detergent belt associated with the RC protein on both the electrostatic environment and the protein lability. Our results show that this influence causes a faster conformational relaxation for LDAO-solubilized RCs than for RCs with either Triton X-100 or Na cholate. The results of the theoretical modeling, given in Table 1 (see Materials and Methods), yield a larger structural diffusion constant for the sample solubilized with LDAO than for those using other detergents, providing good agreement with experimental findings.

CONCLUSION

The experimental and theoretical analysis of the self-consistent behavior of the flow of photoactivated electrons and slow structural motions of photosynthetic RCs performed in this work provides evidence that RCs function as a nonlinear dynamic system. The results obtained for equilibration kinetics of RCs as a function of light conditions favor their description as a nonequilibrium system with a light-dependent shape of the adiabatic conformational potential.

In the present work, the first observation of the dependence of RCs equilibration kinetics on actinic light intensity switching interval times is presented. The theoretical modeling of the effect allows attributing it to the nonlinear dynamic effect of equilibration of RC population between two valleys of a double-well generalized conformational potential. The experiments with actinic pulses applied to intensively preilluminated samples show that the slow relaxation component is most probably an indicator of RCs with highly deformed structures. These structural changes were shown to be induced by lengthy adaptation of RCs to high-intensity actinic light. Comparison of experimental and theoretical results allow for determination of the conformational potential parameters for RCs isolated with different detergents.

The authors thank Dr. N.I. Zakharova and Dr. N. Woodbury for the samples they generously provided for these studies.

Partial support from the Volkswagenstiftung, Hannover, Germany (Schwerpunkt program ''Intra and Intermolecular Electron Transfer in Chemistry and Biology,'' project No. 1/73491), the Ukrainian Foundation for Fundamental Research, and the Committee on Research at the University of California/Riverside is gratefully acknowledged.

REFERENCES

Abgaryan, G. A., L. N. Christophorov, A. O. Goushcha, A. R. Holzwarth, V. N. Kharkyanen, P. P. Knox, and E. A. Lukashev. 1998. Effects of mutual influence of photoinduced electron transitions and slow structural rearrangements in bacterial photosynthetic reaction centers. *J. Biol. Phys.* 24:1–17.

Agmon, N. 2000. Conformational cycle of a single working enzyme. *J. Phys. Chem. B.* 104:7830–7834.

Agmon, N., and J. J. Hopfield. 1983. CO binding to heme proteins: a model for barrier height distributions and slow conformational changes. *J. Chem. Phys.* 79:2042–2053.

Agmon, N., and E. B. Krissinel. 1998. Incoherent control of protein conformational state. *Chem. Phys. Lett.* 294:79–86.

Agostiano, A., F. Milano, and M. Trotta. 1999. Investigation on the detergent role in the function of secondary quinone in bacterial reaction centers. *Eur. J. Biochem.* 262:358–364.

Barabash, Y. M., N. M. Berezetskaya, L. N. Christophorov, A. O. Goushcha, and V. N. Kharkyanen. 2002. Effects of structural memory in protein reactions. *J. Chem. Phys.* 116:4339–4352.

Carpintero, G., and H. Lamela. 2000. Nonlinear dynamics pose challenge and opportunity. *Laser Focus World.* 36:137–140.

Chinarov, V. A., Y. B. Gaididei, V. N. Kharkyanen, and S. P. Sit'ko. 1992. Ion pores in biological membranes as self-organized bistable systems. *Phys. Rev. A.* 46:5232–5241.

Christophorov, L., A. Holzwarth, V. N. Kharkyanen, and F. van Mourik. 2000. Structure-function self-organization in nonequilibrium macromolecular systems. *Chem. Phys.* 256:45–60.

Christophorov, L. N., V. N. Kharkyanen, and S. P. Sit'ko. 1992. On the concept of the non-equilibrium conformon. *J. Biol. Phys.* 18:191–202.

Feher, G., and M. Y. Okamura. 1978. Chemical composition and properties of reaction centers. *In* The Photosynthetic Bacteria. R.K. Clayton, and W.R. Sistrom, editors. Plenum Press, New York. 349–386.

Frauenfelder, H., S. G. Sligar, and P. G. Wolynes. 1991. The energy landscapes and motions of proteins. *Science*. 254:1598–1603.

Gast, P., P. W. Hemelrijk, H. J. van Gorkom, and A. J. Hoff. 1996. The association of different detergents with the photosynthetic reaction center protein of Rhodobacter sphaeroides R26 and the effects on its photochemistry. *Eur. J. Biochem.* 239:805–809.

Goushcha, A. O., A. R. Holzwarth, and V. N. Kharkyanen. 1999. Self-regulation phenomenon of electronic-conformational transitions in biological electron transfer under non-equilibrium conditions. *Phys. Rev. E.* 59:3444–3452.

Goushcha, A. O., M. T. Kapoustina, V. N. Kharkyanen, and A. R. Holzwarth. 1997a. Nonlinear dynamic processes in an ensemble of photosynthetic reaction centers. Theory and experiment. *J. Phys. Chem. B.* 101:7612–7619.

Goushcha, A. O., V. N. Kharkyanen, and A. R. Holzwarth. 1997b. Nonlinear light-induced properties of photosynthetic reaction centers under low intensity irradiation. *J. Phys. Chem. B.* 101:259–265.

Goushcha, A. O., V. N. Kharkyanen, G. W. Scott, and A. R. Holzwarth. 2000. Self-regulation phenomena in bacterial reaction centers. 1. General theory. *Biophys. J.* 79:1237–1252.

Gushcha, A. O., A. A. Dobrovolskii, M. T. Kapoustina, A. V. Privalko, and V. N. Kharkyanen. 1994. New physical phenomenon of dynamical self-organization in molecular electron transfer systems. *Phys. Letters A.* 191:393–397.

Haken, H. 1983. Advanced Synergetics. Springer-Verlag, New York.

Hoff, A. J., and J. Deisenhofer. 1997. Photophysics of photosynthesis. structure and spectroscopy of reaction centers of purple bacteria. *Phys. Rep.* 297:1–247.

Kleinfeld, D., M. Y. Okamura, and G. Feher. 1984. Electron transfer kinetics in photosynthetic reaction centers cooled to cryogenic temperatures in the charge-separated state: evidence of light-induced structural changes. *Biochemistry.* 23:5780–5786.

Lin, S., E. Katilius, A. L. M. Haffa, A. K. W. Taguchi, and N. W. Woodbury. 2001. Blue light drives B-side electron transfer in bacterial photosynthetic reaction centers. *Biochemistry.* 40:13767–13773.

Marone, P. A., P. Thiyagarajan, A. M. Wagner, and D. M. Tiede. 1999. Effect of detergent alkyl chain length on crystallization of a detergent-solubilized membrane protein: correlation of protein-detergent particle size and particle-particle interaction with crystallization of the photosynthetic reaction center from Rhodobacter sphaeroides. *J. Crystal Growth.* 207:214–225.

McMahon, B. H., J. D. Müller, C. A. Wraight, and G. U. Nienhaus. 1998. Electron transfer and protein dynamics in photosynthetic reaction center. *Biophys. J.* 74:2567–2587.

Michel, H. 1991. Properties of commonly used non-ionic and zwitterionic detergents for membrane protein solubilization and crystallization. *In* Crystallization of Membrane Proteins. H. Michel, editor. CRC Press, Boston. 209–211.

Nicolis, G., and I. Prigogine. 1977. Self Organization in Nonequilibrium Systems. Wiley, New York.

Rosso, L., P. Minary, Z. Zhu, and M. E. Tuckerman. 2002. On the use of the adiabatic molecular dynamics technique in the calculation of free energy profiles. *J. Chem. Phys.* 116:4389–4402.

Ruan, X., J. Wei, Q. Xu, J. S. Wang, Y. D. Gong, X. F. Zhang, T. Y. Kuang, and N. M. Zhao. 2000. Comparison of the effects of Triton X-100 treatment on the protein secondary structure of Photosystem I and Photosystem II studied by FT-IR spectroscopy. *J. Mol. Struct.* 525:97–106.

Shinkarev, V. P., and C. A. Wraight. 1997. The interaction of quinone and detergent with reaction centers of purple bacteria. I. Slow quinone exchange between reaction center micelles and pure detergent micelles. *Biophys. J.* 72:2304–2319.

Tiede, D. M., L. Utchig, D. K. Hanson, and D. M. Gallo. 1998. Resolution of electron and proton transfer events in the electrochromism associated with quinone reduction in bacterial reaction centers. *Photosynth. Res.* 55:267–273.

Tiede, D. M., J. Vazquez, J. Cordova, and P. A. Marone. 1996. Time-resolved electrochromism associated with the formation of quinone anions in the Rhodobacter sphaeroides R26 reaction center. *Biochemistry.* 35:10763–10775.

Tributsch, H., and R. A. Bogomolni. 1994. Bacteriorhodopsin—a molecular photooscillator. *Chem. Phys. Lett.* 227:74–78.

Tributsch, H., and L. Pohlmann. 1992. Far from equilibrium cooperative electron transfer—the energetic advantage. *Chem. Phys. Lett.* 188: 338–342.

Tributsch, H., and L. Pohlmann. 1998. Electron transfer: classical approaches and new frontiers. *Science.* 279:1891–1895.

Van Mourik, F., M. Reus, and A. R. Holzwarth. 2001. Long-lived charge separated states in bacterial reaction centers isolated from Rhodobacter sphaeroides. *Biochim. Biophys. Acta.* 1504:311–318.

Valerio-Lepiniec, M., J. D. Delcroix, M. Schijer, D. K. Hanson, and P. Sebban. 1997. A native electrostatic environment near Q(B) is not sufficient to ensure rapid proton delivery in photosynthetic reaction centers. *FEBS Lett.* 407:159–163.

Warshel, A., and W. W. Parson. 2001. Dynamics of biochemical and biophysical reactions: insight from computer simulations. *Q. Rev. Biophys.* 34:563–679.

Zakharova, N. I., and I. Y. Churbanova. 2000. Methods of isolation of reaction center preparations from photosynthetic purple bacteria. *Biochemistry.* 65:181–193.

Zakharova, N. I., M. Fabian, N. Ia. Uspenskaia, A. A. Kononenko, and A. B. Rubin. 1981. Structural-functional characteristics of photosynthetic reaction centers extracted by treatment with lauryldimethylamine oxide from Rhodopseudomonas sphaeroides (wild type). *Biokhimiia.* 46: 1703–1711.